Materials Research. 2014; 17(6): 1449-1465
DOI: http://dx.doi.org/10.1590/1516-1439.289014

Corrosion Resistance of 2024 Aluminum Alloy Coated with Plasma Deposited a-C:H:Si:O Films

***Daniela Branco Tavares Mascagni*[a]*, Maria Eliziane Pires de Souza*[a], *Celia Marina de Alvarenga Freire*[b], *Selma Luiza Silva*[c], *Rita de Cássia Cipriano Rangel*[a], *Nilson Cristino da Cruz*[a], *Elidiane Cipriano Rangel*[a]**

[a]*Laboratory of Technological Plasmas, Paulista State University – UNESP, Experimental Campus of Sorocaba, Sorocaba, SP, Brazil*
[b]*Department of Materials Engineering, University of Campinas – UNICAMP, Campinas, SP, Brazil*
[c]*Centro Tecnológico da Marinha em São Paulo – ARAMAR, Iperó, SP, Brazil*

Received: April 8, 2014 – Revised: November 30, 2014

AA 2024 aluminum alloy is widely employed in aeronautic and automobilist industries. Its hardness and low density are attractive properties for such industrial areas. However, since it contains copper, it undergoes severe corrosion in aggressive media as saline or low Earth orbit environments. In this work, it was investigated the properties of films deposited by PECVD on AA 2024 aluminum alloy as well as the corrosion resistance of the film/substrate systems under different corrosive atmospheres. Films were prepared in a plasma atmosphere composed of 50% of oxygen and 50% of hexamethyldisiloxane resulting in a total gas pressure of 4.0 Pa. Plasma ignition was promoted by the application of radiofrequency signal (13.56 MHz) to the sample holder while grounding the topmost electrode. The plasma excitation power, P, was changed from 10 to 80 W in the six different set of experiments. Film thickness, measured by profilometer, increases by 5 times as P was elevated from 10 to 80 W. As demonstrated by the infrared spectra of the samples, films are essentially organosilicons with preservation of functional groups of the precursor molecule and with creation of different ones. The oxide proportion and the structure crosslinking degree are affected by the plasma excitation power. According to the results obtained by sessile drop technique, hydrophilic to moderately hydrophobic films are produced with changing P from 10 to 80 W. The corrosion resistance, evaluated by salt spray and electrochemical impedance spectroscopy, EIS, experiments, in general increases after film deposition. It is demonstrated that film deposition improves, in up to 36 times, the resistance of the alloy to salt spray attack. It is also shown an improvement of about 240 times in the alloy resistance under NaCl solution by the EIS data. Micrographs acquired by Scanning Electron Microscopy after the corrosion tests furnish further information on the importance of the layer physical stability on its barrier properties. Furthermore, films highly protect the alloy against the oxygen attack. Interpretations are proposed based on the modification of the plasma kinetics with P, altering film structure, composition and properties.

Keywords: *PECVD, plasma treatment, corrosion protection, 2024 aluminum alloy*

1. Introduction

Al 2024-T3, a heterogeneous Al–Cu alloy containing 4.5% of Cu[1], is a high strength alloy widely employed in aerospace industry[2]. The strength of this material is a consequence of precipitates formed by addition of copper but this incorporation also turns the alloy susceptive to galvanic corrosion[1], particularly when in contact with chloride-containing[2] and oxygen rich environments. Therefore, improvements on the corrosion resistance of this material are mandatory to enhance its performance in practical applications[3]. Barrier layers grown on metallic surface are recognized as a way to avoid interactions of the corrosive medium and surface species and then the oxidative process. Films deposited from the activation of precursors by glow discharges (PECVD) appears as in interesting alternative[4] since their physical and chemical properties can be tailored by the plasma excitation parameters[6]. The deposition process is free of toxic solvents and chromates[5,6], dry, clean, fast, relatively inexpensive and easy to perform. Furthermore, it provides uniform, homogeneous and pinhole-free coatings, very convenient characteristics as one considers barrier properties.

Organosilicon to oxide films can be deposited by PECVD from hexamethyldisiloxane, HMDSO[5,7-9]. The deposition kinetics is based on the HMDSO fragmentation and multiple step reactions in the plasma phase, providing precursors for film formation[7]. When O_2 is added to the vapor of HMDSO (HMDSO/O_2), organic constituents are

*e-mail: danibtmascagni@gmail.com

scavenged from the films, increasing the inorganic character (SiO_2-like)[5,10] of the structure. This change improves the film adhesion to aluminum substrates[6] and when associated with an increase in the plasma excitation power, produces relatively more cross-linked[11] and then denser structures, interesting features as one considers a barrier layer. The application of plasma films as protective layers on metals[12,13] has already been reported, especially those prepared from HDMSO. It has been demonstrated that such films present a relatively higher performance because of the affinity of Si towards various metals, mainly aluminum alloys[14]. Furthermore, besides being resistant to chemical attacks, organosilicon or silica-like plasma deposited films can have their physical properties adjusted by controlling the plasma excitation parameters.

In this work, it was investigated the effect of the plasma excitation power on the chemical composition, molecular structure, water wettability of films deposited from HMDSO and O_2 mixtures on 2024 aluminum alloy. The performance of the film-substrate under saline environments and oxygen rich atmosphere was also accessed.

2. Experimental

25 x 25 x 9 mm^3 mirror finish polished AA 2024 T3 plates were cleaned in cycles of 600 s in ultrasonic baths using a detergent solution for aluminum, distilled water and isopropyl alcohol. Afterwards, the samples were dried in a hot air flow and placed on the lower electrode of the plasma reactor, Figure 1, which was fully described elsewhere[12]. The system was evacuated down to 2.0 Pa and argon was admitted until the pressure to reach 15 Pa. The plasma, maintained for 600 s, was generated by the application of radiofrequency, RF, power (13.56 MHz, 70 W) to the sample holder (lower electrode) to sputter clear the substrate surfaces. The deposition process was subsequently conducted for 3600 s in radiofrequency plasmas of 50% of O_2 and 50% of HDMSO at a fixed pressure of 4.0 Pa. The plasma excitation power was varied from 10 to 80 W.

The chemical structure of the films was evaluated by infrared reflectance absorbance spectroscopy (IRRAS) using a Jasco FTIR 410 system. The presented spectra correspond to the average of 128 scannings collected with a resolution of 4 cm^{-1}. The thicknesses of the films were determined with a surface profilemeter (Veeco, Dektak 150). To perform the measurements, the films were deposited on a glass slide containing a Kapton tape mask (5413, 3M) to protect half of its surface from deposition. The height of the step, measured with the aid of the profilemeter, corresponds to the film thickness. For each sample, thickness was measured for at least 10 times in different regions of the step. The wettability of the films was analyzed using 2 µL deionized water droplets in a goniometer (Ramé-Hart 100 and RHI 2001 image program). Three readings were acquired in different positions of the surface.

The resistance of the films to oxidation was derived from the etching rate in reactive oxygen plasmas. Samples prepared on glass plates were partially masked by another glass plate and submitted to the corrosion RF plasma (13.56 MHz, 50 W, 2.0 Pa) for 1800 s. The plasma attack promoted a step between the unprotected and masked regions. The ratio between the step height (thickness of the etched layer) and the exposure time to the plasma, furnishes the etching rate. In this case, thickness measurements were performed 10 times in each sample.

The EIS tests were conducted in a 3.5 wt.% NaCl solution, using a cell with three electrodes: the working electrode (sample), reference electrode (saturated calomel electrode) and the counter electrode (platinum). The applied signal, 10 mV in amplitude, was varied in frequency from 10^{-2} to 10^5 Hz, using a potentiostat (PAR Model 273A) connected to a lock-in (PAR Model 5210), and a software for data acquisition (PAR Electrochemistry Power Suite).

The salt spray tests were carried out in a chamber (Corrotest CA-680, Druckman) in accordance with ASTM B117-07a.

Micrographs of the samples were obtained prior and after the impedance tests, in a scanning electron microscope (SEM) (XL30 – Philips) using the backscattered electron detector and beam energies of 15.0 kV and 20.0 kV. The semi-quantitative elemental composition of the films

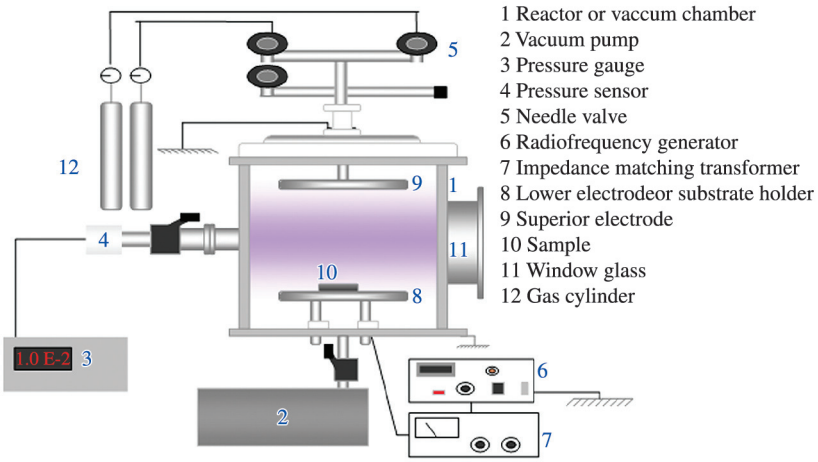

Figure 1. Experimental setup used for film deposition and substrate cleaning by sputtering.

was evaluated by energy dispersive spectroscopy system (XL40-Edax), coupled to the SEM. The regions most affected by the impedance tests were selected for the inspections.

3. Results and Discussions

3.1. Thickness

Figure 2 shows the thickness, h, of the films as a function of P. In general, the thickness increases but at two different growing rates depending on the P range. In both cases, growth occurs almost linearly with power.

According to these results deposition rate increases from 4.8 to 42.6 nm.min^{-1} in the P range investigated here. Similar results were obtained in a previous work[15] using a higher pressure (20 Pa) but with no oxygen addition in the gas mixture. The films deposited with the discharge power exceeding 50 W kept only a few hours adhered to the substrates. However, it is important to emphasize that films as thick as 2.0 μm were obtained with good physical stability.

The thickness trend can be explained by the influence of the plasma excitation power on the intrinsic discharge parameters. As P is augmented, the amplitude of the applied electrical field enhances, increasing the force acting on charged species[16]. As one considers that the same pressure conditions were maintained in all the experiments, the mean energy of the plasma species thus increases, turning the activation of neutrals more effective. Amongst others, the amount of the organosilicon molecule fragments available in the plasma grows, enhancing the availability of film precursors. Deposition rate increases consequently.

Furthermore, with increasing P, there is rise in the self-bias potential, V_b. It is known that the self-bias is directly proportional to $P^{1/2}$ and inversely proportional to $p^{(1/2)}$[17], where p is the plasma pressure. The negative bias generated in the driven electrode attracts positive ions from the glow, promoting ion bombardment of the samples. With increasing V_b, the energy and dose of ions impinging on the growing structure increase, creating extra active sites. Defects (vacancies, ad atoms and clusters) production upon ion bombardment are recognized as responsible for the increment in the concentration of nucleation points[18] where fragments can deposit, thus enhancing deposition rate.

3.2. Molecular structure

Figure 3 shows the infrared spectra of films deposited using two different oxygen proportions in the plasma feed: 0 and 50%. The wavenumber of the main absorption bands were collected and identified in Table 1, according to other relevant studies[10,11,19-25]. The spectra revealed the presence of asymmetric (2950 cm^{-1}) and symmetric (2900 cm^{-1}) C-H stretching vibrations. Methylsilil groups were also identified by the bands lying at 1408 cm^{-1} (asymmetric deformation of CH_3 in $(Si(CH_3)_x)$, around 1200 cm^{-1} (symmetric deformation of CH_3 in $Si(CH_3)_x$) and 800-850 cm^{-1} (stretching and rotation of CH_3 in $Si(CH_3)_x$). The absorptions around 1080-1020 cm^{-1} revealed the presence of Si-O-Si groups, characteristic of the original organosilicon compound ($(CH_3)_3$-Si-O-Si-$(CH_3)_3$). It was also detected

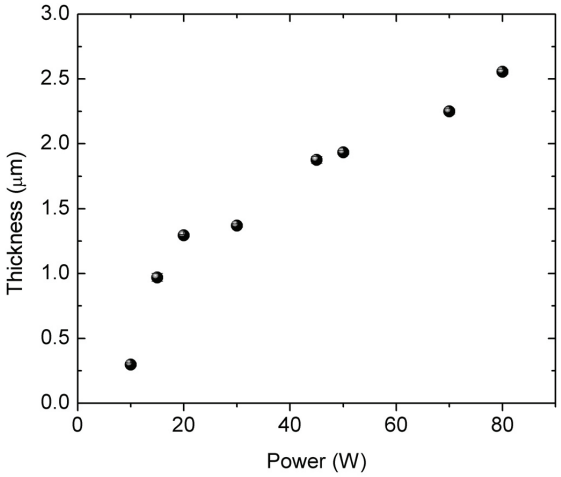

Figure 2. Thickness of the films as a function of power for discharges composed of 50% of HMDSO and 50% of O_2.

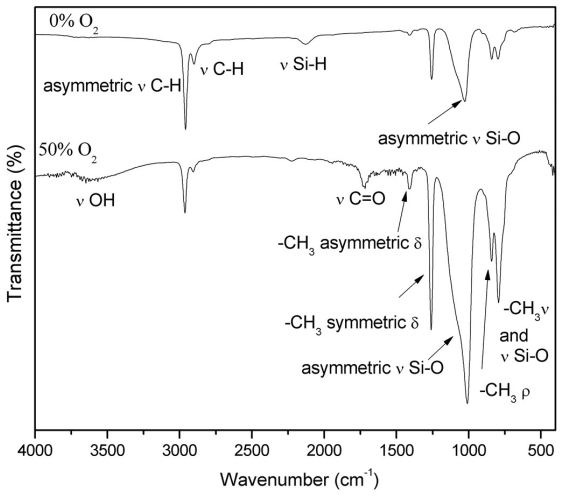

Figure 3. Infrared spectra of films deposited in plasmas with 0 and 50% of oxygen. The ν, δ and ρ symbols mean stretching, deformation and rotation, respectively.

Table 1. Absorption bands detected in the infrared spectra of plasma-polymerized films from pure HMDSO or using equal proportions of HMDSO and O_2 in the gas mixture.

Wavenumber (cm^{-1})	Mode
3645	OH ν in free SiOH[19]
2960	C-H asymmetric ν in CH_3[20]
2900	C-H symmetric ν in CH_3[10]
2200	Si-H ν[21]
1710	C=O[21]
1408	CH_3asymmetric δ in $Si(CH_3)x$[22,24]
1257	CH_3symmetric δ in Si-$(CH_3)_x$[23-25]
1080-1020	Si-O asymmetric ν in Si-O-Si[24]
1027	Si-O asymmetric ν in Si-O-Si and Si-O-C[25]
839	-CH_3ρ in Si-$(CH_3)_3$[11]
790-800	-CH_3ν in Si-$(CH_3)_2$ and Si-O in ν Si-O-Si[23]

the Si-H (2200 cm^{-1}) functional that is not recognized in the original organic compound, suggesting its formation by multiple step reactions in the plasma phase.

In the spectrum of the film derived from HMDSO/O_2 plasma mixture it is possible to observe a broad absorption centered at 3645 cm^{-1} relative to O-H stretching mode in SiOH group[19] as well as an absorption at 1710 cm^{-1} associated with the C=O stretching mode[21]. Both contributions were not detected in the spectrum of the film prepared from pure HMDSO since they are not present in the original organosilicon molecule, corroborating the proposal of multiple step reactions in the plasma phase. Finally, it should be pointed out the strong influence of oxygen on the oxide content of the film structure. There is evidence of silica enrichment as one compares the C-H/Si-O intensity ratio for the bands at 2960 and 1027 cm^{-1}. In the first spectrum, this ratio is 1.78 while in the second it drops to 0.3.

The infrared spectra of the films deposited from HMDSO/O_2 mixture using different excitation powers, depicted in Figure 4, reveal the same absorptions previously listed in Table 1. The prominent and sharp band in the spectra, characteristic of the methylsilil vibration, appears around 1260 cm^{-1}. With increasing power from 10 to 80 W, the intensity of the band at 1080 cm^{-1} (Si-O-Si) growths with respect to that at 1030 cm^{-1}, indicating variations in the SiO_x stoichiometry, with x approaching two[23]. There is a rise of news bands lying at 1354 cm^{-1} (-CH_2 scissors in $Si(CH_2)Si$[24,25]) and 890 cm^{-1} (-CH_3 rotation in $Si(CH_3)_2$)[10], indicating further fragmentation of the starting organosilicon monomer with increasing P. Furthermore, bands at 3645 cm^{-1} (OH stretching) assigned to silanol groups[19] develop in the spectra as P is elevated.

Considering the evolution of the absorption band around 1240 cm^{-1} it is possible to infer about the crosslinking degree of the chains[26,27]. This band can be decomposed in the mono-substituted (M), di-substituted (D) and tri-substituted (T) SiO functional. The absorption at 1255 cm^{-1} is assigned to the M group, containing three methyls bonded to silicon, SiR_3, corresponding to an end group of the chain. The contribution at 1265 cm^{-1} refers to the D structure; formed by two methyl functional bonded to the silicon network $R_2Si(\text{-O-})_2$. Finally, the absorption at 1275 cm^{-1} is related to the T group consisting of a methyl and three oxygen atoms, $RSi(\text{-O-})_3$. The spectra of Figure 5 shows a clear increment in the contribution of the D and T functional with increasing P. The rise in the proportion of D functional, a propagation unit in the chain, indicates the formation of longer and branched chains, very similar to those found in the conventional polydimethylsiloxane (Figure 6) structure. On the other hand, the rise in the T functional band intensity reveals an oxygen enrichment and a consequent elevation in the crosslinking degree.

3.3. Contact angle

Figure 7 shows the contact angle, θ, of the films as a function of plasma excitation power. Films with different wettabilities were obtained depending on the P. For deposition using the lowest excitation power (10 W), the resulting film is hydrophilic with contact angles below 80°. However, for P ≥ 15 W, θ keeps roughly constant around 95°, thereby, characterizing the films as moderately hydrophobic.

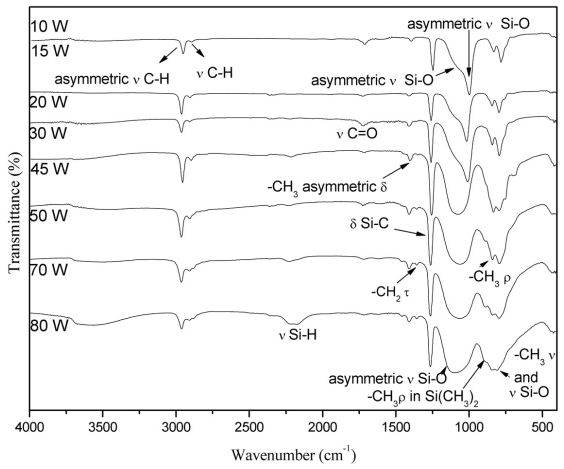

Figure 4. Infrared spectra of films prepared with discharge powers ranging from 10 to 80 W. The symbols ν, δ, ρ and τ mean stretching, deformation, rotation and scissors, respectively.

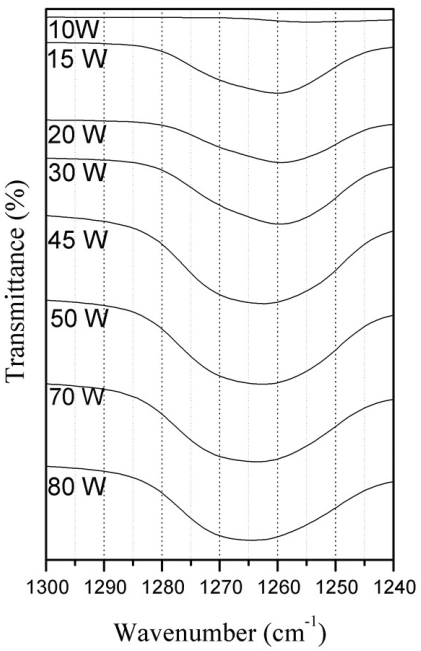

Figure 5. Infrared spectra of the films deposited with powers ranging from 10 to 80 W in the region between 1300 and 1240 cm^{-1}.

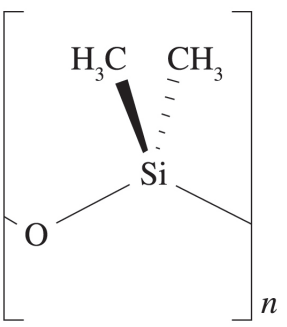

Figure 6. Polydimethylsiloxane structural formula.

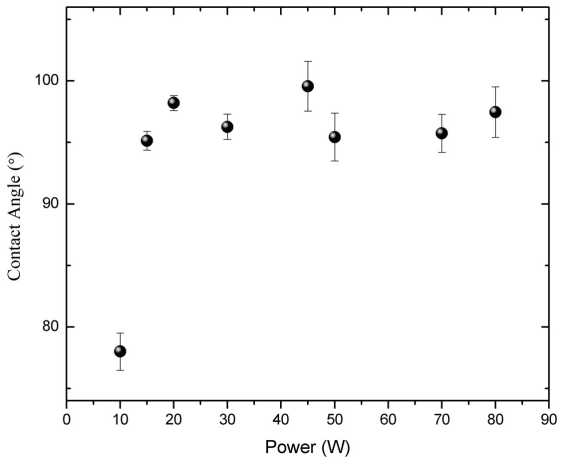

Figure 7. Contact angle of the films as a function of plasma excitation power.

The low wettability of the films is related to the presence of methyl groups attached to the Si-O backbone[22]. Despite the presence of polar Si-O groups in the chains, nonpolar methyl groups shield the electrostatic attraction between the silica and water molecules. This further indicates the formation of an organosilicon structure in which silica groups are surrounded by methyl groups in a way very similar to that observed in conventional polydimethylsiloxane (95-113°)[28]. Finally, the changes detected in the molecular structure with increasing P, were not enough to promote significant changes on the wettability of the films.

3.4. Corrosion resistance

Figure 8 shows the pictures of the uncoated 2024 aluminum alloy before (a) and after (b) the salt spray exposure. Figures 9 to 14 show the equivalent results for the samples containing the films prepared from HMDSO/O_2 plasmas with powers ranging from 10 to 80 W.

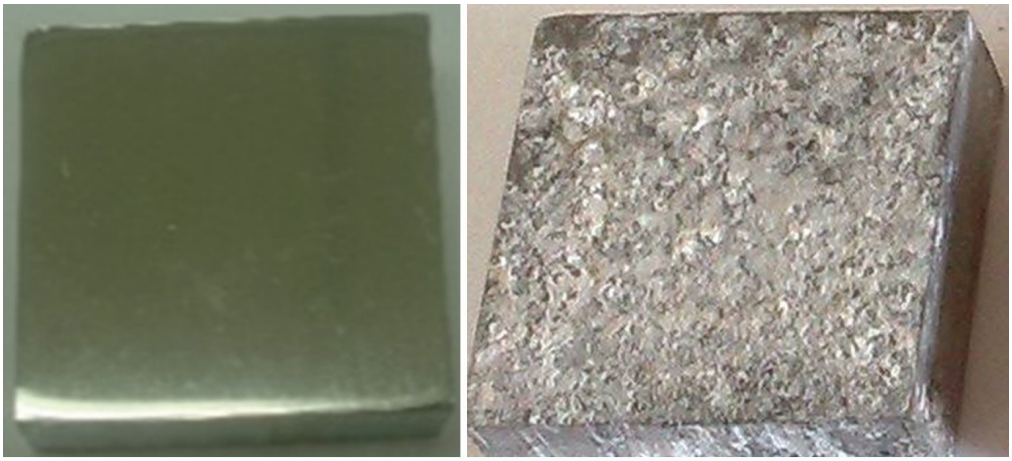

(a) (b)

Figure 8. (a) Surface of the untreated sample before the test and (b) after 145 h of exposure to salt spray.

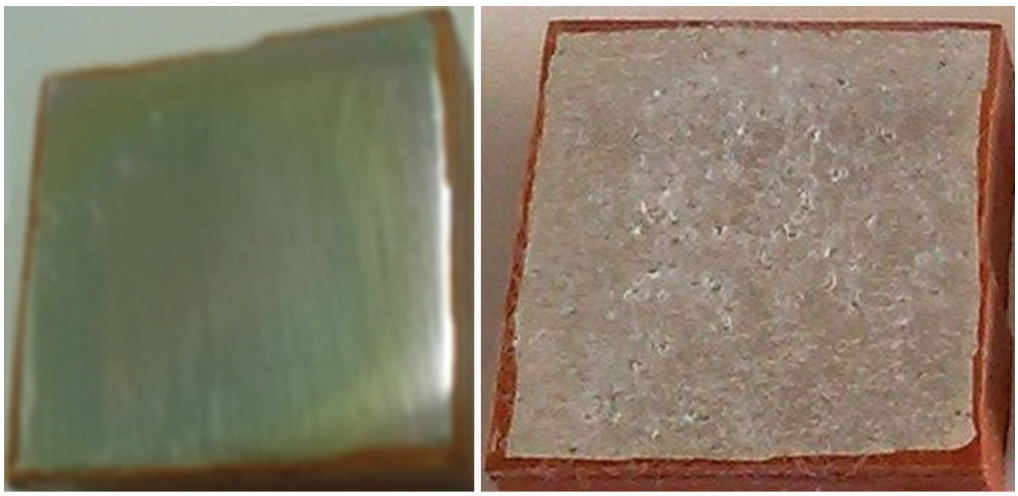

(a) (b)

Figure 9. (a) Surface of the sample containing the film deposited in plasmas of 10 W of power, before the test and (b) after 145 h of exposure to salt spray.

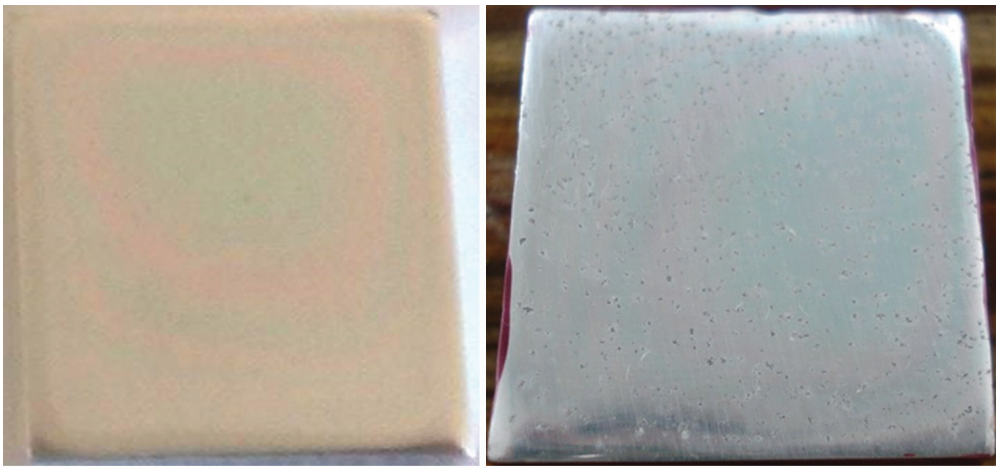

(a) (b)

Figure 10. (a) Surface of the sample containing the film deposited in plasmas of 15 W of power, before the test and (b) after 145 h of exposure to salt spray.

(a) (b)

Figure 11. (a) Surface of the sample containing the film deposited in plasmas of 20 W of power, before the test and (b) after 145 h of exposure to salt spray.

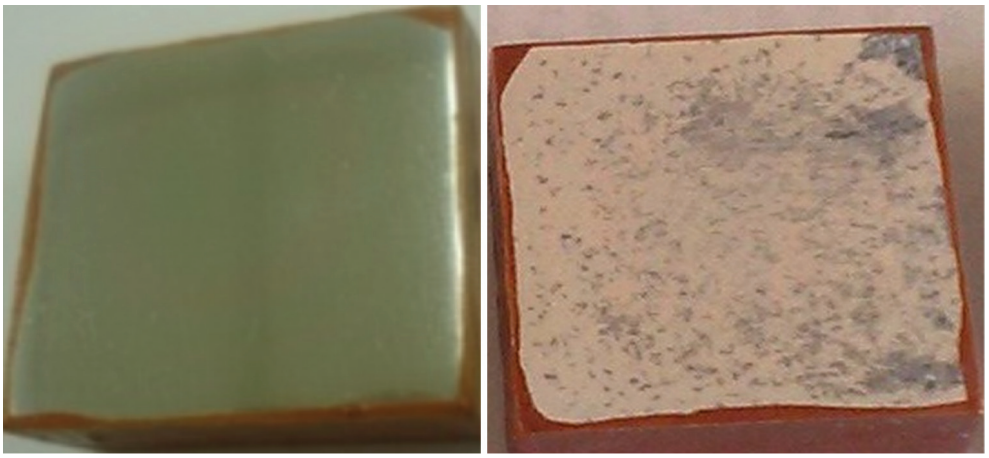

(a) (b)

Figure 12. (a) Surface of the sample containing the film deposited in plasmas of 30 W of power, before the test and (b) after 145 h of exposure to salt spray.

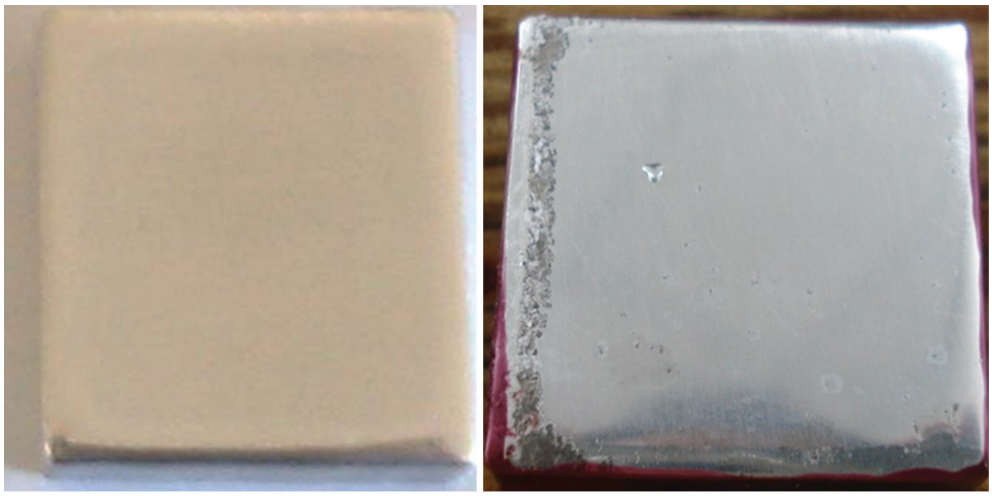

(a) (b)

Figure 13. (a) Surface of the sample containing the film deposited in plasmas of 45 W of power, before the test and (b) after 145 h of exposure to salt spray.

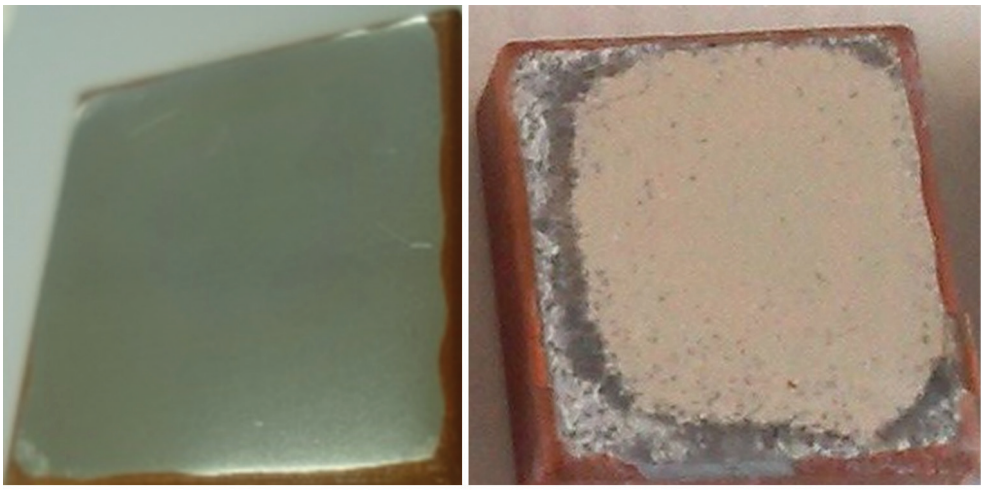

(a) (b)

Figure 14. (a) Surface of the sample containing the film deposited in plasmas of 50 W of power, before the test and (b) after 145 h of exposure to salt spray.

The visual inspection of the uncoated sample that was exposed to the salt spray test reveals general surface corrosion after just 4 h of exposure. After 145 h, the surface degradation is severe (Figure 8). For the samples containing films deposited using $P \leq 30$ W (Figure 9 to Figure 12) a minor protection is obtained since corrosion points appear as pits created by diffusion of oxidative species through the coating. However, for the sample prepared with P = 45 W (Figure 13) the pit concentration is substantially reduced, suggesting a great improvement in the barrier properties. For the system prepared in 50 W plasmas (Figure 14), corrosion at edges compromised the overall physical integrity of the coating. The pits, sparsely dispersed on the entire surface, appear again, indicating loss in the barrier properties.

Thus, the thickness increase (Figure 2) influences the corrosion performance in two opposite ways: it improves the barrier properties but also increases the chances of punctual detachment under saline atmosphere (or solution), since the internal tension rises with thickness[16]. Another relevant aspect is the rise in the silanol (SiOH) proportion with increasing P from 45 to 50 W (Figure 4). The incorporation of these groups creates points in the structure with high affinity towards water molecules/vapor, which then induces hydrolysis and eventually deteriorates the film barriers properties[29].

The better performance of the film prepared in plasmas of 45 W, despite its lower thickness, is observed as one compares the images of Figures 13b and 14b: corrosion stopped very near the edges, but with excellent integrity of the center of the sample. Therefore, the film that associated the best physical integrity to the best barrier properties was that prepared in plasmas of 45 W since it enhanced in 36 times the corrosion resistance of the alloy in salt spray environment.

For the EIS results, the dependence of the impedance modulus, $|Z|$, on the applied frequency, allows to separate the response of the system into two different components: the capacitance and resistance of the protective layers. The evolution of these parameters during the corrosion process can be used to distinguish the corrosion protection efficiency of the different coatings. Figure 15 shows the curves of $|Z|$ versus frequency for the films deposited from HMDSO/O_2 on the 2024 alloy.

In general, all the systems present higher impedance at the lowest frequency. With increasing the deposition power, it is observed an up shift of the curves, indicating improvements in the corrosion resistance (R_T). At low frequencies (10^{-1} Hz), the $|Z|$ can be related to the total resistance (R_T) defined as the sum of the electrolyte resistance, polarization resistance and pore resistance, reflecting the overall corrosion resistance. In order to quantify the differences of the coatings, the total resistance was determined and is depicted in Figure 16 as a function of P. The corresponding value for the bare Al 2024 alloy is represented as a dashed line in this graph.

The bare aluminum alloy itself presents a high total resistance (~10^4 Ω) compared to the bare carbon steel (~10^2 Ω)[15]. As the film is deposited, R_t in general grows but at different rates, depending on the power used for preparing the films. The fastest growth occurs with increasing P from 10 to 20 W, with the establishment of a plateau (~ 7X10^6 Ω) for P≥ 30 W. These results show a strict correspondence with the thickness ones in which a sudden elevations was observed for the same P range. However, for moderate to high powers (> 20 W) thickness enhancement does not affect any longer the barrier properties. This result is attributed to a balance between the improvement in the barrier properties and the deterioration in the physical stability of the films activated by the elevation in h. Even though a branched and crosslinked structure with higher oxide contents had been obtained at higher powers, there was also increment in the proportion of silanol groups hindering further improvements. Interestingly, corrosion resistance increased 240 times as films deposited with moderated powers (30-50 W) were applied on the 2024 aluminum alloy.

The total capacitance, C_T, of the systems, was calculated by the extrapolation of the $|Z|$ curve from frequencies between 10^1-10^3 Hz to 10^{-1} Hz[30]. Figure 17 shows the results as a function of P. The dashed line in this graph represents the total capacitance for the bare alloy. For the sample containing the film deposited at the lowest power (10 W) C_t was even higher than the observed in the bare alloy. Nevertheless, a steep decline in C_T (about two orders of magnitude) is detected as power is increased from 10 to 15 W. This behavior is consistent with a pronounced increase in thickness (~ 4 times) and impedance modulus (> 10 times) in the same range of power. However, no further changes in C_t are observed with increasing power from 15 to 45 W, although the total resistance and the film thickness had varied significantly for this power range. Finally, with increasing P beyond 45 W produces a new downward trend (~ 10 times) in C_T, which cannot be explained only by changes in impedance and thickness of the films, which were very mild in this case. Indeed, the correspondence between the impedance and capacitance with thickness was observed only for the 10 to 15 W

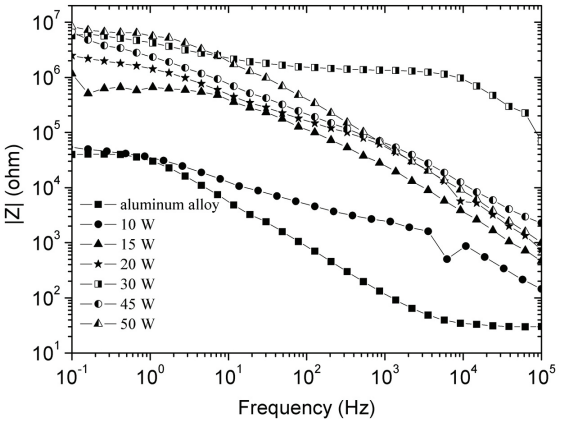

Figure 15. Impedance modulus versus frequency for the films deposited from HMDSO/O_2 on the 2024 Al alloy using discharge powers ranging from 10 to 50 W.

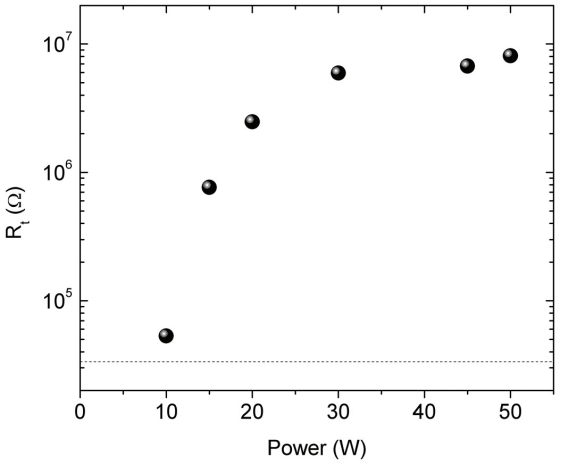

Figure 16. Total resistance as a functions of the plasma deposition power for the films deposited from HMDSO/O_2 on the 2024 alloy. Dashed line corresponds to the total resistance for the uncoated polished alloy.

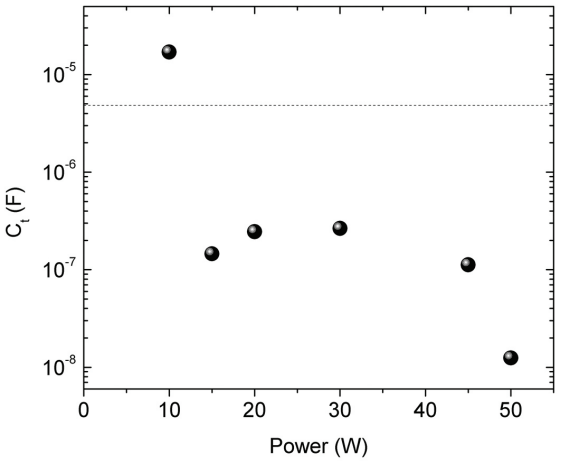

Figure 17. Total capacitance as a function of P for films deposited from HMDSO/O_2 with plasma excitation powers ranging from 10 to 50 W. Dashed line corresponds to the uncoated polished alloy.

power ranges. The threshold for which thickness trends cannot explain the C_T behavior any longer, is ascribed to the compositional and structural changes, since it was for P > 30 W, that major structural and compositional changes were detected in the films. Therefore, considering the C_t results, the film that promoted the best protection to the alloy, decreasing around 390 times the total capacitance, was that prepared with 50 W.

In order to evaluate the effect of the corrosion on the surface of the samples, scanning electron micrographs were generated after the EIS tests. Figure 18 shows the micrograph of the polished bare alloy as well as the energy dispersive spectra generated from the points marked in the micrograph. In the Table 2 are the results of the semi-quantitative analysis.

In the micrograph it is possible to identify an uniform matrix (region C) rich in Al, with Cu as an alloying element, in good agreement with the results reported in literature for the 2024 aluminum alloy[31]. In this material, small dark (region A) and white (region B) incrustations are immersed. While the first (region A) is rich in Si and O, but otherwise poor in Al, the second (region B) presents Mn and Fe in its constitution[31].

Figures 19 to 24 show the aspect of the plasma coated surfaces after the EIS experiments. The surface is composed by two different granular structures. The first one is the same

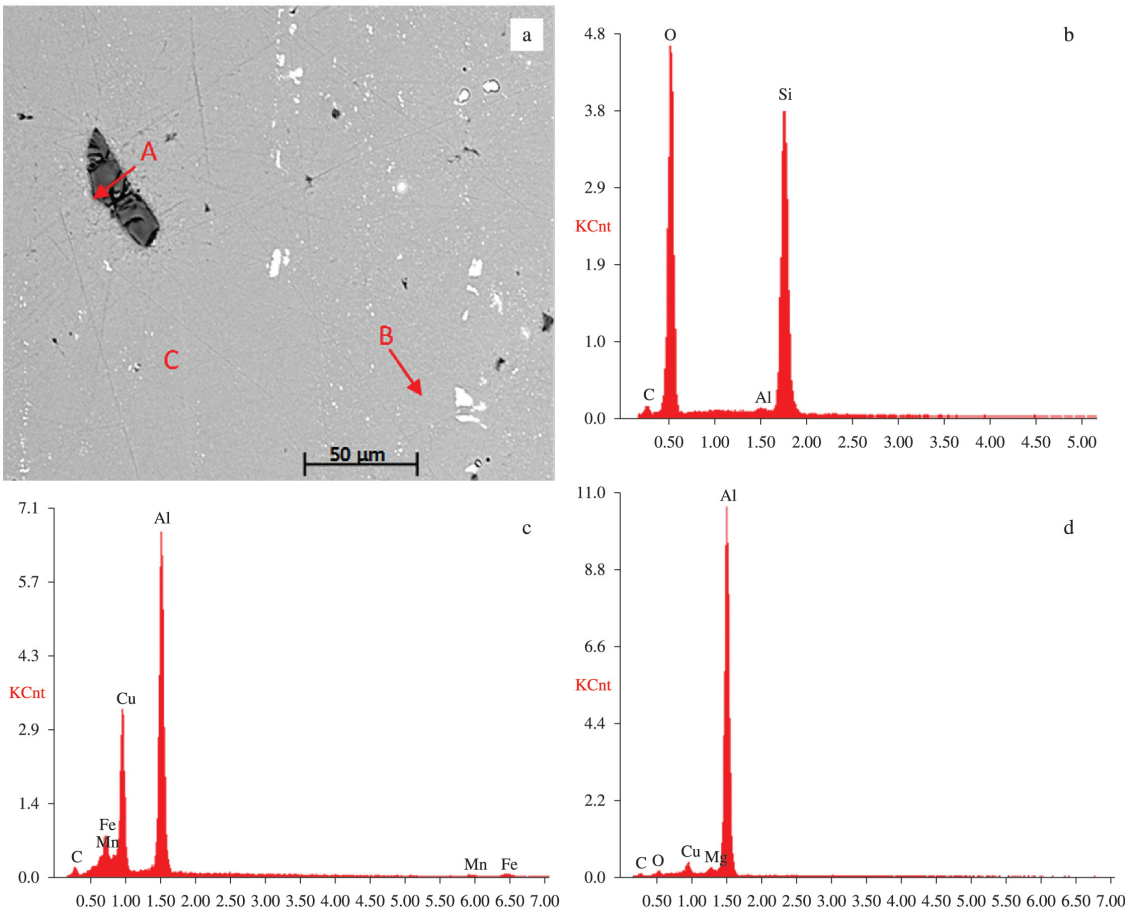

Figure 18. (a) Scanning electron micrograph of the uncoated aluminum. A (b), B (c) and C (d) are energy dispersive spectra taken from regions A, B and C marked in the micrograph.

Table 2. Results for the semi-quantitative analysis of 2024 aluminum alloy.

Semi-quantitative region A			Semi-quantitative region B			Semi-quantitative region C		
Element	**Weight (%)**	**Atomic (%)**	**Element**	**Weight (%)**	**Atomic (%)**	**Element**	**Weight (%)**	**Atomic (%)**
C K	5.97	9.73	C K	6.10	16.85	C K	5.23	11.18
O K	47.09	57.57	Cu L	32.22	16.82	O K	1.65	2.65
Al K	0.55	0.40	Al K	46.65	57.36	Cu K	4.94	2.00
Si K	46.38	32.30	Mn K	3.88	2.34	Mg K	1.97	2.08
-	-	-	Fe K	11.15	6.63	Al K	86.22	82.10
Total	100.00	100.00	Total	Total	100.00	Total	100.00	100.00

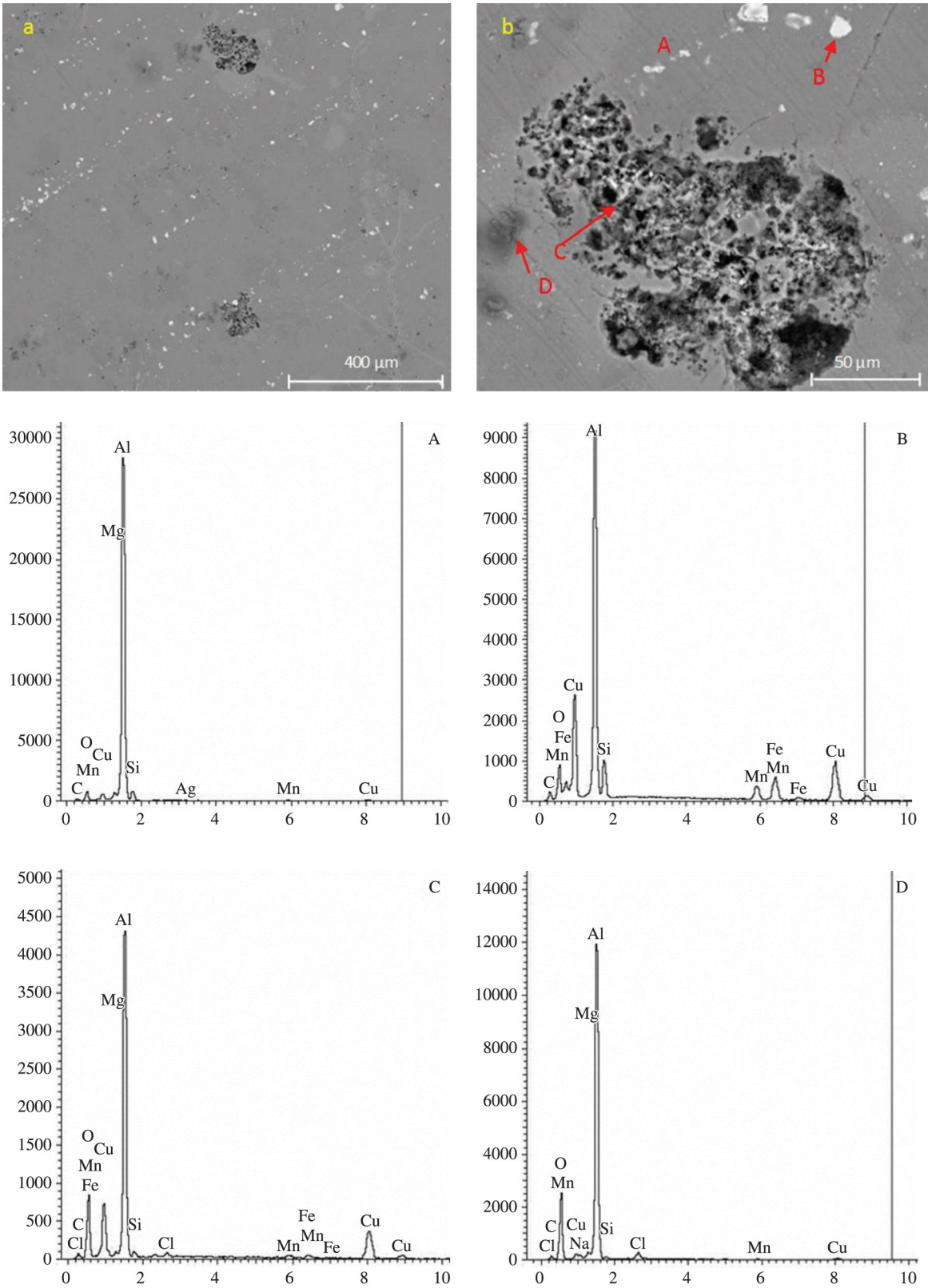

Figure 19. Scanning electron micrograph of the sample containing the film deposited with discharge power of 10 W with amplification of (a) 250 times and (b) 1500 times. A, B, C and D are energy dispersive spectra of the regions A, B, C and D of the micrograph shown in (b).

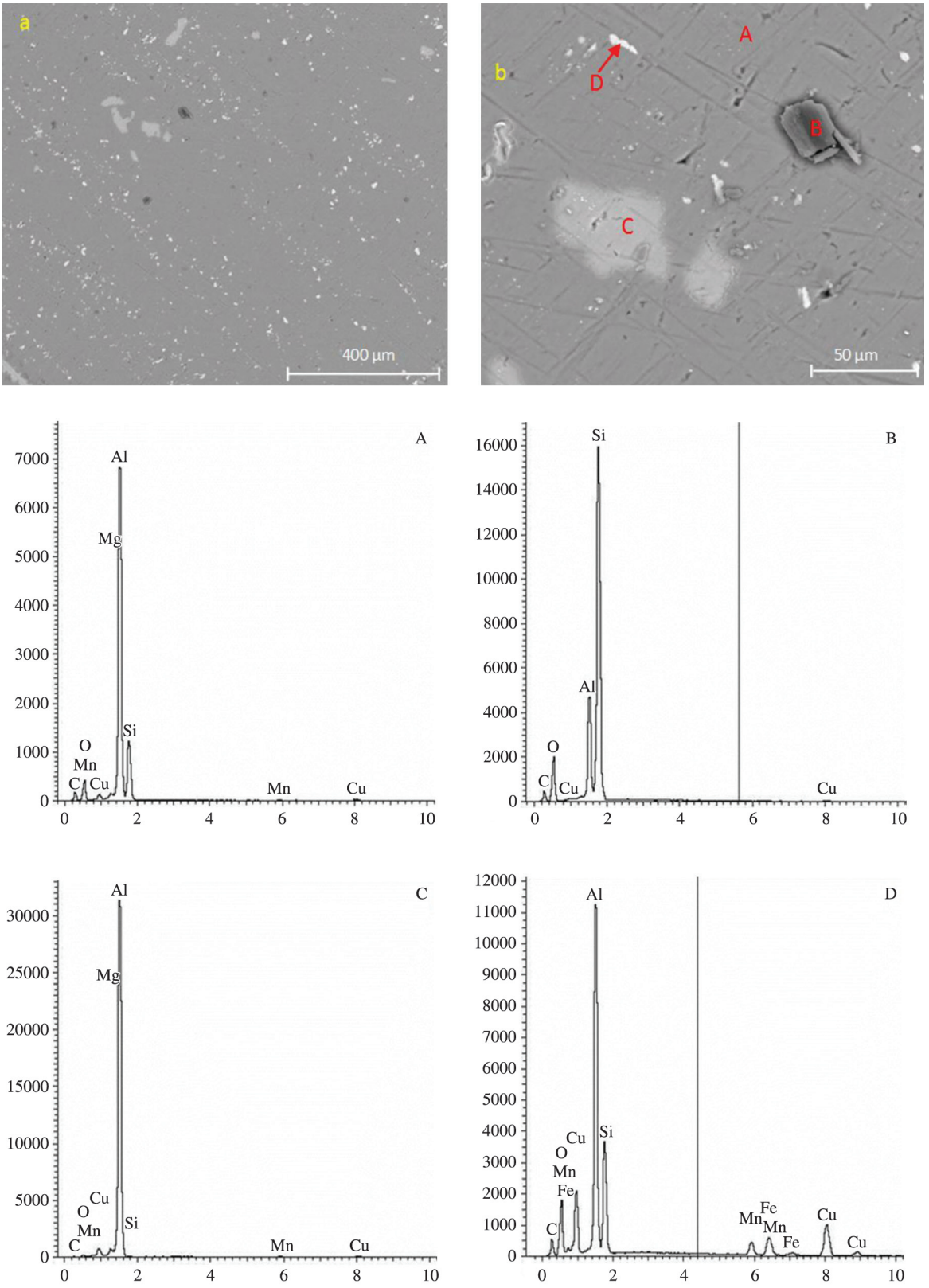

Figure 20. Scanning electron micrograph of the sample containing the film deposited with discharge power of 15 W with amplification of (a) 250 times and (b) 1500 times. A, B, C and D are energy dispersive spectra of the regions A, B, C and D of the micrograph shown in (b).

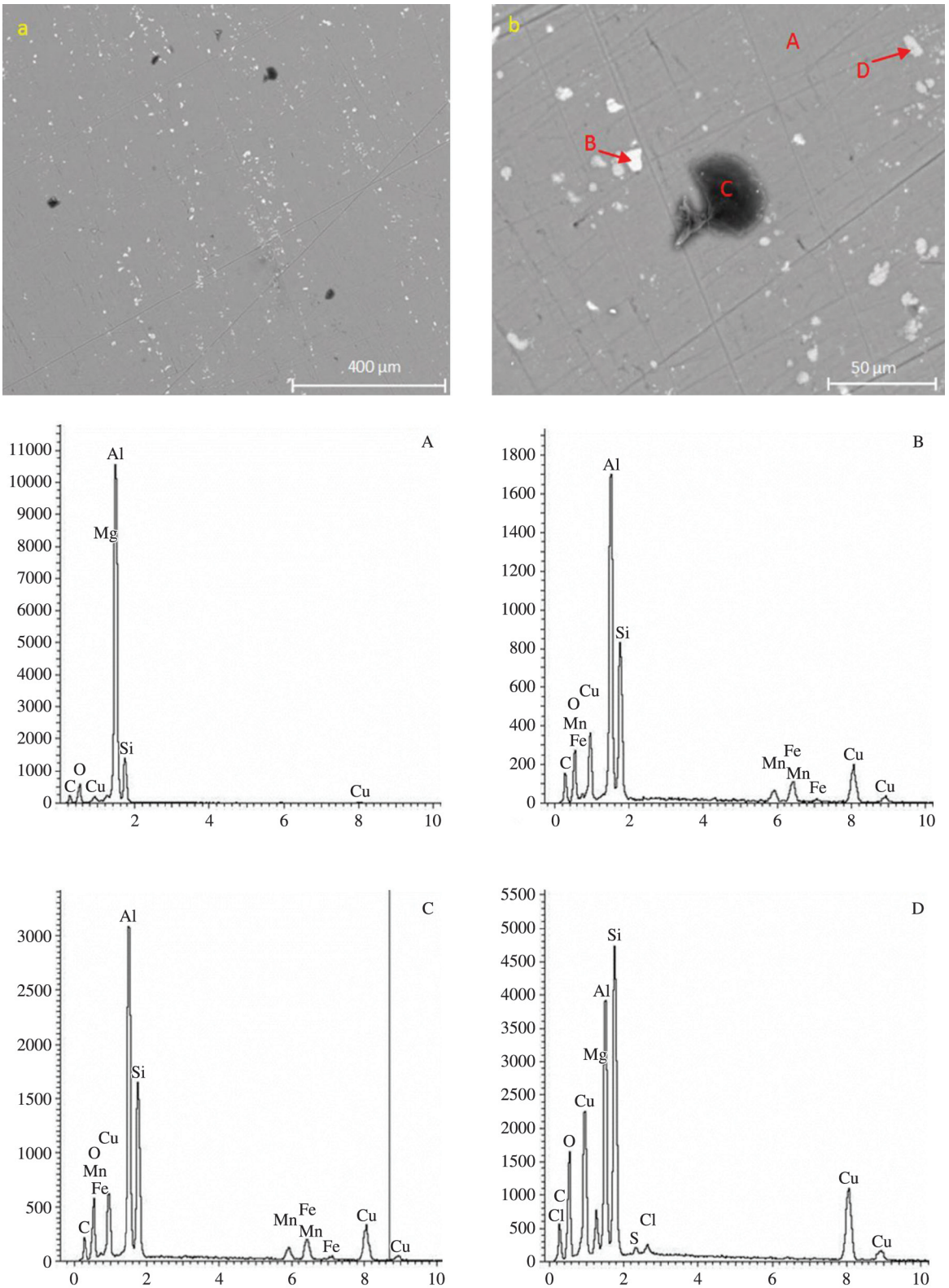

Figure 21. Scanning electron micrograph of the sample containing the film deposited with discharge power of 20 W with amplification of (a) 250 times and (b) 1500 times. A, B, C and D are energy dispersive spectra of the regions A, B, C and D of the micrograph shown in (b).

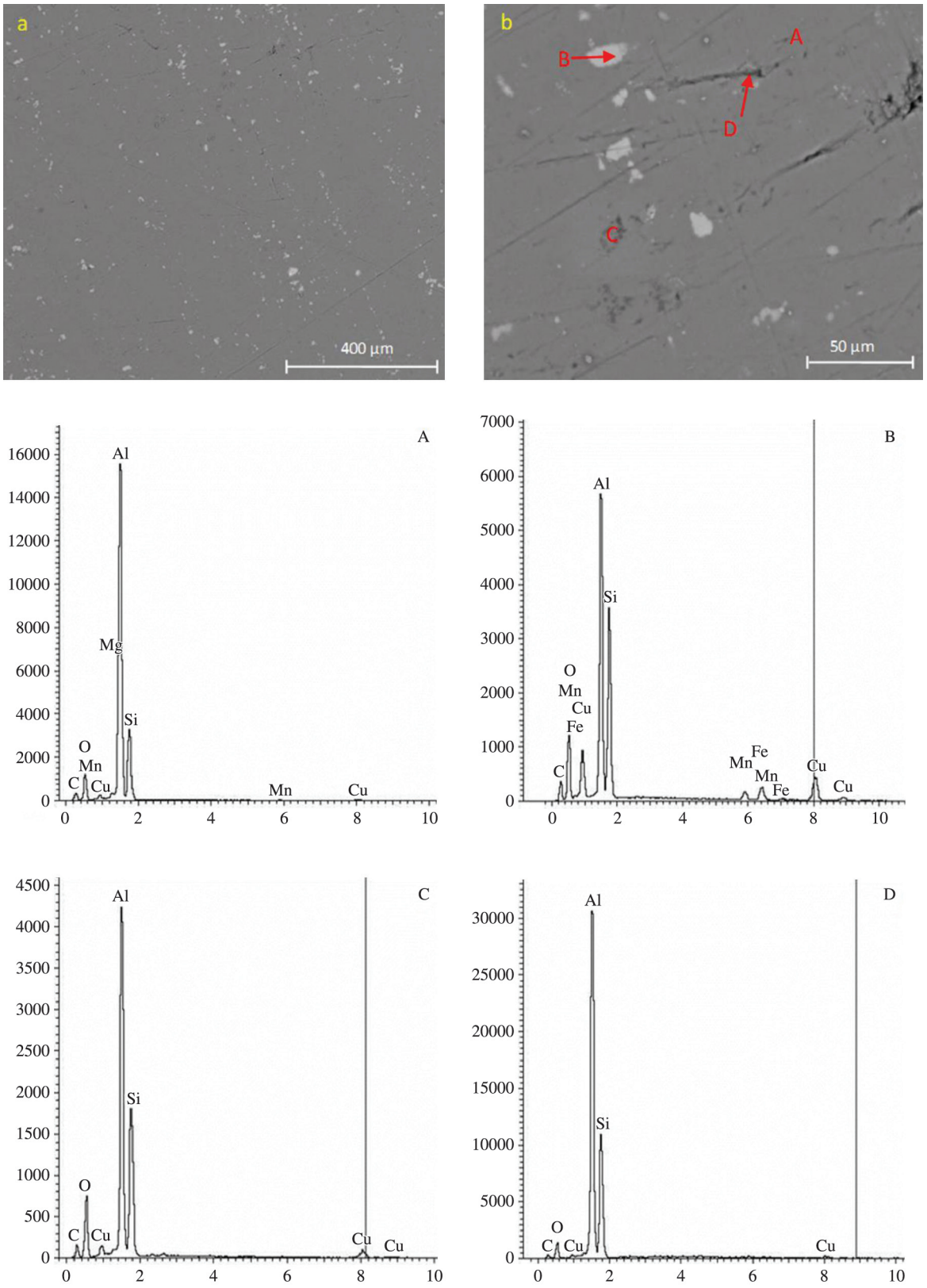

Figure 22. Scanning electron micrograph of the sample containing the film deposited with discharge power of 30 W with amplification of (a) 250 times and (b) 1500 times. A, B, C and D are energy dispersive spectra of the regions A, B, C and D of the micrograph shown in (b).

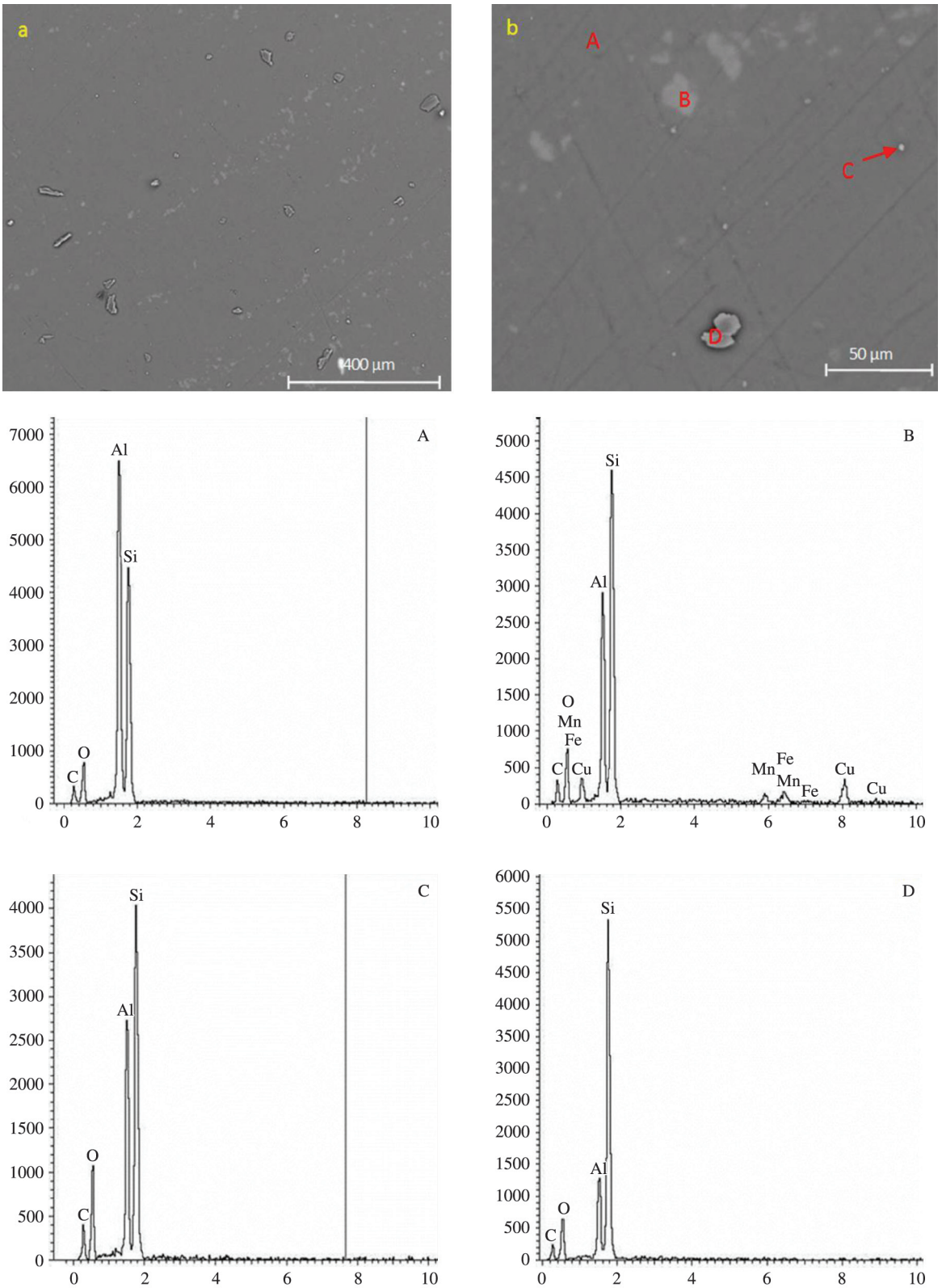

Figure 23. Scanning electron micrograph of the sample containing the film deposited with discharge power of 45 W with amplification of (a) 250 times and (b) 1500 times. A, B, C and D are energy dispersive spectra of the regions A, B, C and D of the micrograph shown in (b).

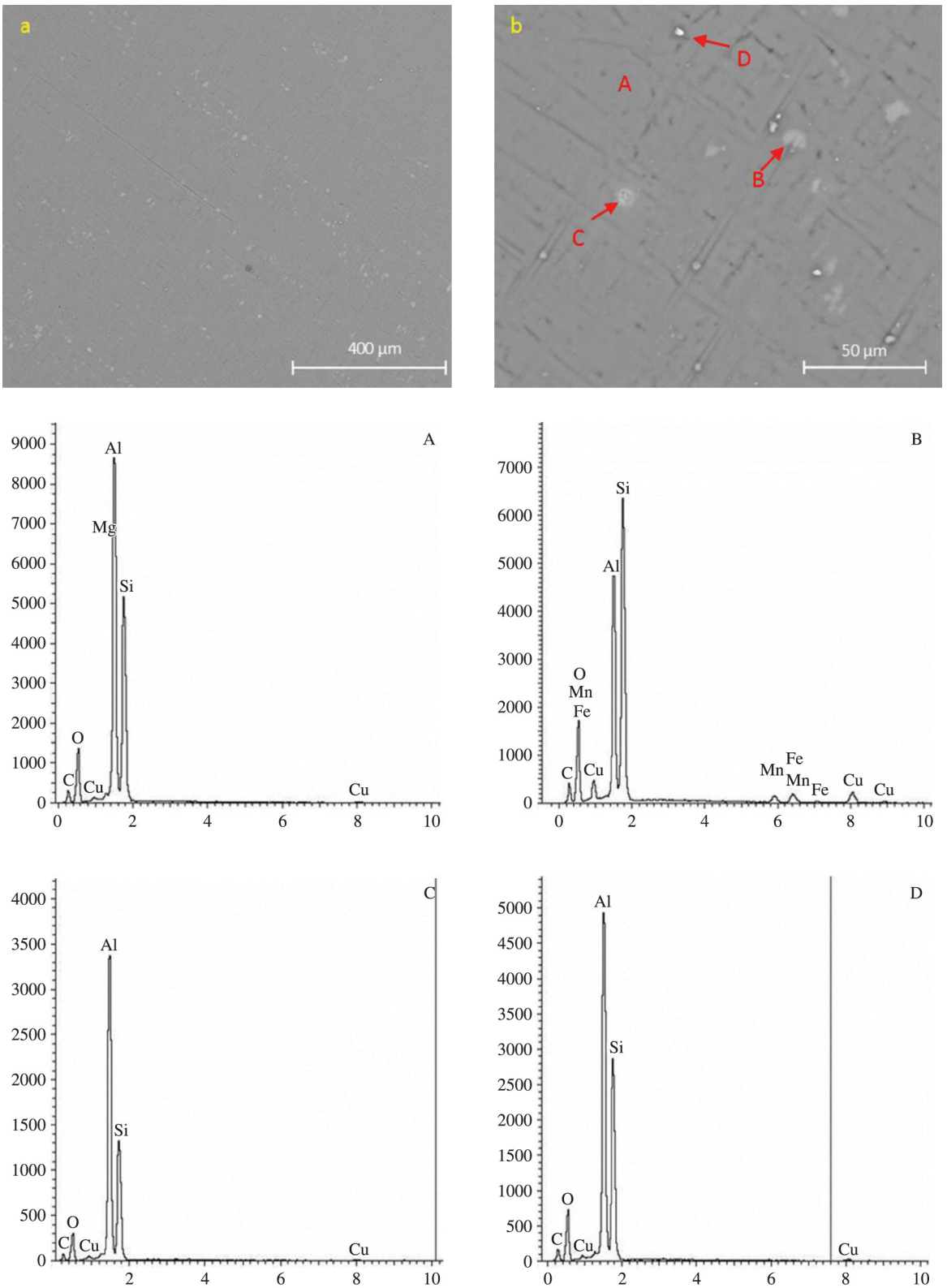

Figure 24. Scanning electron micrograph of the sample containing the film deposited with discharge power of 50 W with amplification of (a) 250 times and (b) 1500 times. A, B, C and D are energy dispersive spectra of the regions A, B, C and D of the micrograph shown in (b).

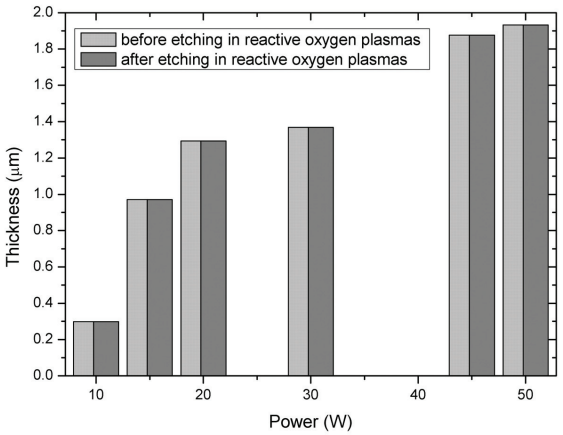

Figure 25. Thickness of the films before and after etching in reactive oxygen plasma as a function of the depositing plasma power.

irregular particle observed in the bare material, originating from the own alloy constitution (Table 2). The second one is a regular spherical structure smaller than the first. In general, the concentration of this spherical white spots (region C of Figure 23), composed of silicon, oxygen and carbon and normally observed in organosilicon films deposited from plasmas of HMDSO[19], increases after film deposition. This kind of structure, formed by polymerization in the plasma phase, is demonstrated to strongly depend on the oxygen proportion in the plasma phase and on the deposition time[32]. In the present work, the concentration of the polymeric spots increases with power up to 15 W, but it decreases afterwards. The scratches, rising from the bare polished alloy, are still identified after film deposition, mainly in the samples containing the thinner films ($P \leq 30$ W). These regions, represented by the D area of the Figure 24b, have a lower Si concentration.

Craters, originated from the corrosion procedure, appear in the sample treated with the lowest plasma power (Figure 19b). Around such defects, a white shadow is always present, as also illustrated in the C region of Figure 20b. This region shows a low Si concentration and then reflects points where film was partially removed by reaction with the saline solution. These two corrosion induced defects were detected mainly in the samples with the thinnest films (10 and 15 W). For the others, there was preservation of the layer even after interaction with the solution.

Figure 25 shows the thickness of the layers prior and after exposure to ablation in reactive oxygen plasmas. Interestingly, the thickness of the layer removed by the plasma ablation was not detected by perfilometry. Considering that resolution of the profilemeter employed here is better than 100 Å, little material was removed from the surface despite the high affinity of oxygen towards the organic part of the structure. Therefore, the etching rate of the films was considered null in all the cases. This result, also observed in a previous study[15], is ascribed to the oxidation of the very first atomic layers of the films with intense loss of methyl groups, resulting in an oxide top layer. This one, very resistant to the atomic oxygen attack, protects the underneath organosilicon bulk from further ablation. This result becomes especially interesting as one considers the applicability of the 2024 aluminum alloy in aerospace devices.

4. Conclusions

In this work, hydrophobic, physically stable and relatively thick a-C:H:Si:O films were deposited from HMDSO/O_2 plasma mixture on the 2024 aluminum alloy. The structure crosslinking degree and the oxide proportion were observed too dependent on the plasma excitation power. Under salt spray atmosphere, films prepared with moderate excitation powers (45 W) increased in up to 36 times the corrosion resistance of the alloy whereas in the electrochemical tests the improvement was more than two orders of magnitude (30-50 W). These improvements are entirely ascribed to the organosilicon coating once the native oxide layer was removed before film deposition. Interestingly, the etching rate upon reactive oxygen attack was null, independently of the employed deposition condition, demonstrating the potentiality of such coatings for protection of aerospace devices.

Acknowledgments

The authors thank Capes and Fapesp for financial support, Prof. Dr. Antonio Junior Riul for technical support and Centro Tecnológico da Marinha em São Paulo – ARAMAR.

References

1. Schneider O and Kelly RG. Localized coating failure of epoxy-coated aluminium alloy 2024-T3 in 0.5M NaCl solutions: Correlation between coating degradation, blister formation and local chemistry within blisters. *Corrosion Science*. 2007; 49(2):594-619. http://dx.doi.org/10.1016/j.corsci.2006.06.006.
2. Fonseca IT, Lima N, Rodrigues JA, Pereira MIS, Salvador JCS and Ferreira MGS. Passivity breakdown of Al 2024-T3 alloy in chloride solutions: a test of the point defect model. *Electrochemistry Communications*. 2002; 4(5):353-357. http://dx.doi.org/10.1016/S1388-2481(02)00273-4.
3. Campestrini P, Van Westing EPM, Hovestad A and De Wit JHW. Investigation of the chromate conversion coating on Alclad 2024 aluminium alloy: effect of the pH of the chromate bath. *Electrochimica Acta*. 2002; 47(7):1097-1113. http://dx.doi.org/10.1016/S0013-4686(01)00818-0.
4. Chan Y and Yu Q. Electrochemical characterization of plasma polymer coatings in corrosion protection of aluminum alloys. *Journal of Vacuum Science & Technology. A, Vacuum, Surfaces, and Films*. 2005; 23(4):991. http://dx.doi.org/10.1116/1.1924716.
5. Azioune A, Marcozzi M, Revello V and Pireaux J-J. Deposition of polysiloxane-like nanofilms onto an aluminium alloy by plasma polymerized hexamethyldisiloxane: characterization by XPS and contact angle measurements. *Surface and Interface Analysis*. 2007; 39(7):615-623. http://dx.doi.org/10.1002/sia.2563.
6. Domingues L, Oliveira C, Fernandes JCS and Ferreira MGS. EIS on plasma-polymerised coatings used as pre-treatment for

aluminium alloys. *Electrochimica Acta*. 2002; 47(13-14):2253-2258. http://dx.doi.org/10.1016/S0013-4686(02)00064-6.

7. Fanelli F, d'Agostino R and Fracassi F. GC-MS Investigation of Hexamethyldisiloxane-Oxygen Fed Cold Plasmas: Low Pressure Versus Atmospheric Pressure Operation. *Plasma Processes and Polymers*. 2011; 8(10):932-941. http://dx.doi.org/10.1002/ppap.201000201.
8. Chaiwong C, Rachtanapun P, Sarapirom S and Boonyawan D. Plasma polymerization of hexamethyldisiloxane: Investigation of the effect of carrier gas related to the film properties. *Surface and Coatings Technology*. 2013; 229:12-17. http://dx.doi.org/10.1016/j.surfcoat.2012.08.058.
9. Patel RP and Wolden CA. Plasma-enhanced chemical vapor deposition synthesis of silica-silicone nanolaminates using a single precursor. *Journal of Vacuum Science & Technology A, Vacuum, Surfaces, and Films*. 2011; 29(2):021012. http://dx.doi.org/10.1116/1.3553149.
10. Benıtez F, Martınez E and Esteve J. Improvement of hardness in plasma polymerized hexamethyldisiloxane coatings by silica-like surface modification. *Thin Solid Films*. 2000; 377-378:109-114. http://dx.doi.org/10.1016/S0040-6090(00)01393-6.
11. Lee SH and Lee DC. Preparation and characterization of thin films by plasma polymerization of hexamethyldisiloxane. *Thin Solid Films*. 1998; 325(1-2):83-86. http://dx.doi.org/10.1016/S0040-6090(98)00492-1.
12. Rangel RCC, Souza MEP, Schreiner WH, Freire CMA, Rangel EC and Cruz NC. Effect of the fluorination of DLC film on the corrosion protection of aluminum alloy (AA 5052). *Surface and Coatings Technology*. 2010; 204(18-19):3022-3028. http://dx.doi.org/10.1016/j.surfcoat.2010.03.055.
13. Hadinata S-S, Lee M-T, Pan S-J, Tsai W-T, Tai C-Y and Shih C-F. Electrochemical performances of diamond-like carbon coatings on carbon steel, stainless steel, and brass. *Thin Solid Films*. 2013; 529:412-416. http://dx.doi.org/10.1016/j.tsf.2012.05.041.
14. Fernandes JCS, Ferreira MGS, Haddow DB, Goruppa A, Short R and Dixon DG. Plasma-polymerised coatings used as pre-treatment for aluminium alloys. *Surface and Coatings Technology*. 2002; 154(1):8-13. http://dx.doi.org/10.1016/S0257-8972(01)01705-4.
15. Rangel RCC, Pompeu TC, Barros JLS Jr, Antonio CA, Santos NM, Pelici BO, et al. Improvement of the corrosion resistance of carbon steel by plasma deposited thin films. In: Razavi RS, editor. *Recent researches in corrosion evaluation and protection;* 2012. Rijeka: InTech Europe. p. 91-116. http://dx.doi.org/10.5772/34623
16. Yasuda HK. *Plasma polymerization*. New York: Academic Press; 1985.
17. Catherine Y and Couderc P, Electrical characteristics and growth kinetics in discharges used for plasma deposition of amorphous carbon. *Thin Solid Films*. 1986; 144(2):265-280. http://dx.doi.org/10.1016/0040-6090(86)90419-0.
18. Esch S, Bott M, Michely T and Comsa G. Nucleation of homoepitaxial films grown with ion assistance on Pt(111). *Applied Physics Letters*. 1995; 67(21):3209. http://dx.doi.org/10.1063/1.115165.
19. Ricci M, Dorier J.-L, Hollenstein C and Fayet P. Influence of argon and nitrogen admixture in HMDSO/O2 plasmas onto powder formation. *Plasma Processes and Polymers*. 2011; 8(2):108-117. http://dx.doi.org/10.1002/ppap.201000052
20. Montarsolo A, Mossotti R, Innocenti R and Vassallo E. A study on washing resistance of pp-HMDSO films deposited on wool fabrics for anti-pilling purposes. *Surface and Coatings Technology*. 2013; 224:109-113. http://dx.doi.org/10.1016/j.surfcoat.2013.03.007.
21. Ko Y-M, Choe H-C, Jung S-C and Kim B-H. Plasma deposition of a silicone-like layer for the corrosion protection of magnesium. *Progress in Organic Coatings*. 2013; 76(12):1827-1832. http://dx.doi.org/10.1016/j.porgcoat.2013.05.024.
22. Gengenbach TR and Griesser HJ. Post-deposition ageing reactions differ markedly between plasma polymers deposited from siloxane and silazane monomers. *Polymer*. 1999; 40(18):5079-5094. http://dx.doi.org/10.1016/S0032-3861(98)00727-7.
23. Kurosawa S, Choi B-G, Park J-W, Aizawa H, Shim K-B and Yamamoto K. Synthesis and characterization of plasma-polymerized hexamethyldisiloxane films. *Thin Solid Films*. 2006; 506-507:176-179. http://dx.doi.org/10.1016/j.tsf.2005.08.210.
24. Petasch W, Baumgärtner K, Räuchle E and Walker M. Influence of plasma surface treatment on the adhesion of thin films on metals. *Surface and Coatings Technology*. 1993; 59(1-3):301-305. http://dx.doi.org/10.1016/0257-8972(93)90101-S.
25. Wavhal DS, Zhang J, Steen ML and Fisher ER. Investigation of gas phase species and deposition of SiO2 films from HMDSO/O2 plasmas. *Plasma Processes and Polymers*. 2006; 3(3):276-287. http://dx.doi.org/10.1002/ppap.200500140.
26. Casserly TB and Gleason KK. Chemical vapor deposition of organosilicon thin films from methylmethoxysilanes. *Plasma Processes and Polymers*. 2005; 2(9):679-687. http://dx.doi.org/10.1002/ppap.200500055.
27. Coclite AM, Milella A, Palumbo F, Fracassi F and d'Agostino R. Chemical and morphological characterization of low-k dielectric films deposited from hexamethyldisiloxane and ethylene RF glow discharges. *Plasma Processes and Polymers*. 2010; 7(12):1022-1029. http://dx.doi.org/10.1002/ppap.201000091.
28. Bouteau M, Cantin S, Fichet O, Perrot F and Teyssié D. Contribution toward comprehension of contact angle values on single polydimethylsiloxane and poly(ethylene oxide) polymer networks. *Langmuir*. 2010; 26(22):17427-17434. http://dx.doi.org/10.1021/la102384s. PMid:20919692
29. Bruce RL, Lin T, Phaneuf RJ, Oehrlein GS, Bell W, Long B, et al. Molecular structure effects on dry etching behavior of Si-containing resists in oxygen plasma. *Journal of Vacuum Science & Technology B Microelectronics and Nanometer Structures*. 2010; 28(4):751. http://dx.doi.org/10.1116/1.3455496.
30. Mansfeld F. Recording and analysis of AC impedance data for corrosion studies. *Corrosion*. 1981; 37(5):301-307. http://dx.doi.org/10.5006/1.3621688.
31. Huda Z, Taib NI and Zaharinie T. Characterization of 2024-T3: an aerospace aluminum alloy. *Materials Chemistry and Physics*. 2009; 113(2-3):515-517. http://dx.doi.org/10.1016/j.matchemphys.2008.09.050.
32. Trasferetti BC, Davanzo CU and Bica de Moraes MA. Infrared and raman studies on films of organosiloxane networks produced by PECVD. *Macromolecules*. 2004; 37(2):459-466. http://dx.doi.org/10.1021/ma035297a.